

## OPEN ACCESS

## EDITED BY

Yuxuan Ren,  
Fudan University, China

## REVIEWED BY

Giuseppe Brunetti,  
Politecnico di Bari, Italy  
Hussein Sabbah,  
American University of the Middle East, Kuwait

## \*CORRESPONDENCE

A.Y. Bekshaev,  
✉ [bekshaev@onu.edu.ua](mailto:bekshaev@onu.edu.ua)  
J. Zheng,  
✉ [dbzj@netease.com](mailto:dbzj@netease.com)

RECEIVED 12 November 2025

REVISED 25 January 2026

ACCEPTED 26 January 2026

PUBLISHED 18 February 2026

## CITATION

Angelsky OV, Bekshaev AY, Zenkova CY,  
Gavrylyak MS, Maksimyak PP, Maksimyak OP,  
Shchukin S, Zheng J and Cai J (2026)  
Plane-wave scattering by asymmetric  
mesoscale semicylinder: controllable  
formation of multiple interrelated photonic  
nanojets.  
*Front. Phys.* 14:1744525.  
doi: 10.3389/fphy.2026.1744525

## COPYRIGHT

© 2026 Angelsky, Bekshaev, Zenkova,  
Gavrylyak, Maksimyak, Maksimyak, Shchukin,  
Zheng and Cai. This is an open-access article  
distributed under the terms of the [Creative Commons Attribution License \(CC BY\)](https://creativecommons.org/licenses/by/4.0/). The  
use, distribution or reproduction in other  
forums is permitted, provided the original  
author(s) and the copyright owner(s) are  
credited and that the original publication in  
this journal is cited, in accordance with  
accepted academic practice. No use,  
distribution or reproduction is permitted  
which does not comply with these terms.

# Plane-wave scattering by asymmetric mesoscale semicylinder: controllable formation of multiple interrelated photonic nanojets

O. V. Angelsky<sup>1,2</sup>, A. Y. Bekshaev<sup>3\*</sup>, C. Yu. Zenkova<sup>2</sup>,  
M. S. Gavrylyak<sup>2</sup>, P. P. Maksimyak<sup>2</sup>, O. P. Maksimyak<sup>2</sup>,  
S. Shchukin<sup>2</sup>, J. Zheng<sup>1\*</sup> and J. Cai<sup>1</sup>

<sup>1</sup>Research Institute of Zhejiang University-Taizhou, Taizhou, Zhejiang, China, <sup>2</sup>Chernivtsi National University, Chernivtsi, Ukraine, <sup>3</sup>Physics Research Institute, Odesa I.I. Mechnikov National University, Odesa, Ukraine

This work reveals new possibilities for creating controllable photonic nanojets (PNJs) and their complexes, “photonic multijets” (PMJs), characterized by the specific morphological and energy-concentrating properties. These specific light structures can be generated upon scattering a monochromatic plane wave by a mesoscale dielectric semicylinder (SC) with geometric asymmetry (its flat surface is inclined with respect to the incident wave). An output field in the form of PMJ unites several interrelated PNJs of comparable intensities. The main spatial features of the separate PNJs, produced in this process, and their interrelations, are investigated via computer modeling based on the COMSOL Multiphysics environment and finite-difference time-domain (FDTD) method. The number, positions, orientations and intensities of the PNJs depend on the SC size, orientation and dielectric parameters as well as on the exciting-light wavelength. The modeling results show the possibilities for purposeful creation and control of the PMJs with desirable characteristics. In particular, excitation by bi-chromatic light with two different wavelengths enables realization of a passive switching element capable of dynamically altering the electromagnetic field distribution depending on the irradiation spectrum. This can be used for creation of optical splitters and switching devices. Their potential characteristics are discussed as well as the prospects for experimental implementation and applications in optical signal-processing systems.

## KEYWORDS

bichromatic excitation, controllable intensity distribution, dielectric semicylinder, light scattering, optical splitter, optical switch, photonic nanojet

## 1 Introduction

In the past decades, alongside plasmonics, dielectric photonics has been rapidly developing [1], as a branch of research associated with increasing the efficiency of interaction between incident radiation and matter. This domain offers new fruitful opportunities for creating sensor structures, manipulating and controlling

nanoparticles, enhancing the quantum yield of luminescence, and approaches to super-high-resolution optical and terahertz microscopy [1]. The efficiency of corresponding devices, compared to plasmonic systems, is explained by the absence of disadvantages originating from high losses inherent in plasmonic structures [2, 3].

Generally, dielectric photonics is based on the use of optically transparent micro- and nanostructures to create specific conditions for propagation, focusing, and conversion of electromagnetic radiation [4, 5]. Dielectric micro- and nanoparticles, microresonators, waveguides, metasurfaces, *etc.*, realize direct channels to purposeful and highly efficient formation of structured electromagnetic fields across a wide spectral range—from visible to terahertz [4, 6–9]. Controlled resonant effects, such as Mie resonances, make it possible to form directional scattering, concentrating energy in subwavelength regions and implementing the functions of miniature lenses, filters, and sensors [9, 10]. Their unique abilities are employed in integrated photonic devices [5, 6], which find applications in nanometrology, biomedical imaging, quantum and nonlinear photonic technologies, and optical communications [4, 11].

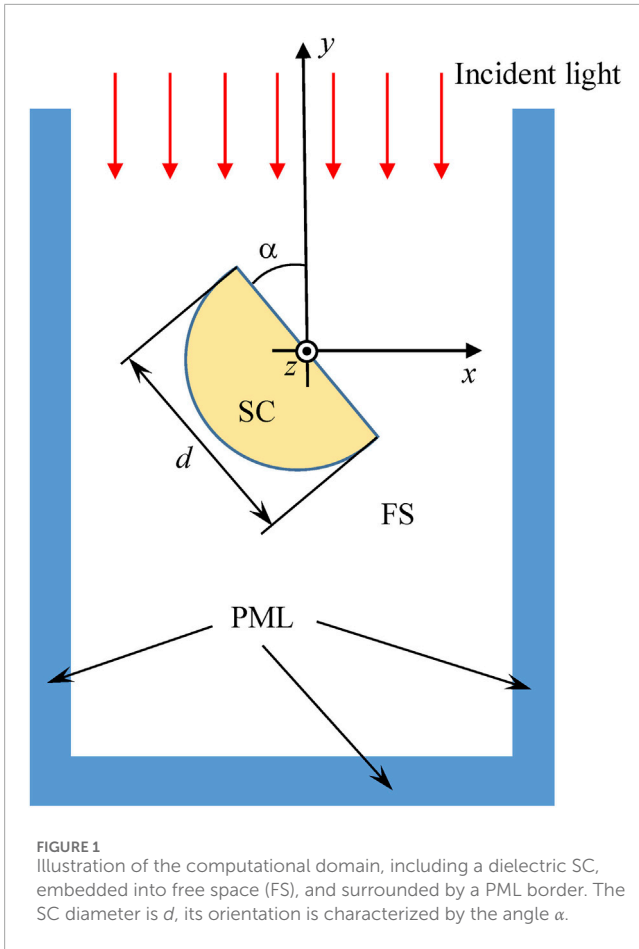
One of the most spectacular manifestations of the principles and achievements of dielectric photonics are photonic nanojets (PNJs)—strictly-localized high-intensity optical beams formed due to the interaction of electromagnetic radiation with dielectric microparticles [7–10, 12–16]. Generally, the PNJs appear as a result of scattering an “exciting” regular wave by transparent particles of various shapes with mesoscale characteristic size (of the order  $\leq 10\lambda$  where  $\lambda$  is the radiation wavelength). In such systems, the geometric-optics phenomena (refraction, reflection, focusing, caustics) are combined with the diffraction, resonance and near-field effects (multipole Mie scattering, whispering-gallery modes, evanescent waves). The corresponding interference processes, involving a lot of interrelated factors, provide extraordinary spatial redistribution of light energy with the formation of narrow focused channels on the shadow side of an illuminated particle [9–16]. In particular, many PNJ structures realize subwavelength energy concentration and focusing a light beam into extremely small areas beneath the usual diffraction limit [4, 10, 12–16], which can be used for probing and optical capture of microscopic objects [4, 11], and for increasing the sensitivity of optical diagnostics [10, 12, 13]. The key parameters of the PNJs: their geometric configuration, length, width, details of the intensity distribution depend on the shape, size, and material of the dielectric micro-object involved. Most commonly, PNJs are formed due to employment of microspheres, cylinders, disks, microprisms made of silicon, glass, quartz, polymers, ceramics as well as some biological materials, including cells and spider silks [4, 6, 13, 17].

Especially interesting features of the PNJ behavior can be observed if the scattering microstructures are of special configurations with broken symmetry [12, 13, 18–23]. These include trapezoids [18, 19], cropped spheres and cylinders, as well as geometrically perfect “patched” particles (with lateral masks attached to their surface) [20, 22], or with specially applied difference in optical properties of their “right” and “left” parts, sometimes called “Janus particles” [20, 23]. Under such conditions, the localized output beams change their direction of propagation due to the action of structure elements of the object, which results in curved PNJ trajectories, thus forming “photonic hooks” (PHs) [18–23]. In essence, PHs represent bent PNJs where the high-intensity region

is concentrated near the curved trajectory; this makes them a near-field counterpart of the paraxial Airy beams [24]. The PHs are unique light structures demonstrating curved trajectories with the radius of curvature reaching subwavelength values ( $<\lambda/2$ ); likewise, the minimal width of a PH can be obtained smaller than the width of a PNJ formed by a symmetric particle, and also lies deep in the subwavelength range ( $<\lambda/2$ ) [19, 20].

In extreme cases, employing mesoscale particles of specially designed complex structure, the PHs may show rather exotic configurations with several bends, loops, *etc.*, [18–20]. In such “deviant” PNJs, a localized propagating PNJ-beam sequentially responds to local phase delays of the interfering contributions, consecutive events of directional scattering and local field enhancement (and, possibly, to local inhomogeneities of the medium) [10, 13, 19, 20, 25]. All these events induce changing the PNJ direction, thus producing a complex spatial field pattern, sometimes of the multilobe nature, which can be termed “photonic zigzag” (PZ) [26]. Important advantages of the PHs is their sensitivity to the scattering conditions (i.e., the particle position, orientation, radiation wavelength, *etc.*) which can be controlled deliberately. As a result, programmable PNJ trajectories can be formed on the subwavelength scale, opening up new possibilities for controlled energy and signal transfer in nanophotonic devices and creation of compact optical circuits for information processing, where PHs act as a kind of “optical router” [4, 25, 27, 28]. That is why PHs are relevant for the development of integrated photonic chips, nanophotonic sensors, and next-generation optical microscopic systems [4, 9, 10, 13, 25, 27, 28].

In the following Sections, a new way for generation and possible application of complex PNJ structures is considered, which is perspective for creation of optical splitters and light switches in optical-communication devices. As a PNJ-generating element, we study a conventional dielectric particle of the semicylinder (SC) shape positioned with geometric asymmetry with respect to the incident (exciting) plane light wave (see Figure 1). Our approach, based on the numerical simulation of the electromagnetic processes in this system, is outlined in Section 2. In Section 3, the main features of the generated PNJs, PHs and associated light-structure components are discussed using the examples of excitation by a plane wave with a wavelength of 632.8 nm. It is shown that the total field pattern contains several interrelated PNJs of comparable intensities which can be considered as a “photonic multijet” (PMJ) structure. The remarkable feature of the PMJ is that its configuration and intensity distributions clearly depend on the scattering conditions: SC size, orientation and the incident-light wavelength. This fact opens the ways for controllable PMJ creation, with desirable positioning of separate PNJs, which can be used, e.g., for the wavelength-dependent switching of the light energy transfer. To estimate the prospects for switching mode of operation, comparative evaluation of the PMJ patterns excited by monochromatic light with two wavelengths,  $\lambda_1 = 1310$  nm and  $\lambda_2 = 1550$  nm, is performed in Section 4. These values are chosen because in these ranges losses in silica fiber are minimal, making them the standard in fiber-optic communication systems [28]; furthermore,  $\lambda_1$  corresponds to zero dispersion in standard fibers, where light pulses propagate without temporal stretching, while  $\lambda_2$  corresponds to minimal loss ( $\sim 0.2$  dB/km) and is often used for long-distance communication lines.



In Section 4, we compare the output field patterns, formed by spatially identical plane waves with the wavelengths  $\lambda_1$  and  $\lambda_2$ , incident on a semi-cylinder of Figure 1. It is revealed that PMJs excited by the  $\lambda_1$ -radiation and  $\lambda_2$ -radiation show specific configurations; some of their spatial features coincide whereas others are clearly distinct. This testifies for the possibility of a selective control of the corresponding light fluxes by changing the wavelengths and the SC orientations, which, in turn, inspires ideas for controllable light splitting and/or routing via transition from  $\lambda_1$  to  $\lambda_2$  and *vice versa*. Some principal capabilities and limitations of hypothetical PMJ-based photonic devices are briefly outlined. In Section 5, we summarize the main regularities of the SC-generated PMJs, possible applications of such structures, and prospects of their further development.

## 2 Mathematical model of the light structure formation by dielectric semycylinder with geometric asymmetry

We consider a PNJ-structure formation in the process of plane-wave scattering at a dielectric particle of the SC shape (Figure 1). The study is performed by means of numerical modeling conducted via COMSOL Multiphysics environment employing the Wave Optics Module [26, 29]. This module provides dedicated tools for

computing the electromagnetic wave propagation and evolution in linear and nonlinear optical media, and enables accurate simulation of the electromagnetic field spatial distribution and optical design optimization.

In our model, the scattering object is a SC, enclosed within the free-space (FS) volume (air/vacuum); to exclude occasional reflection and scattering effects, the whole computational domain is conventionally surrounded by the perfectly-matched absorptive layer (PML) [30]. The SC material is supposed non-magnetic (relative permeability  $\mu_r = 1$ ), but with expressive and adjustable dielectric properties described by real refractive index  $n_r$  or permittivity  $\epsilon_r = n_r^2$ . The SC geometry is characterized by its diameter  $d$  and the plane-face orientation angle  $\alpha$  with respect to the  $y$ -axis, opposite to the incident-wave direction.

It should be noted that characteristics of the PNJs, formed due to scattering at the structure illustrated by Figure 1, are mainly determined by their configuration in the  $(x, y)$ -plane (transverse plane) presented in the figure. We suppose, as usual, that the cylinder length is of the same order of magnitude as its diameter; then, if the incident plane wave propagates perpendicular to the cylinder axis, and if the wave is polarized in the  $z$ -direction, the transverse  $(x, y)$  and longitudinal  $z$  variables are well separated. The specific PNJ features with extraordinary energy concentration and local light amplification are formed in the asymmetric transverse section while the longitudinal effects along the cylinder axis are just usual effects of the strip diffraction. Therefore, analysis of the 2D problem described by Figure 1 is quite informative; possible corrections associated with the longitudinal inhomogeneity have generally rather weak effect on the PNJ spatial structure in the middle SC section (see the brief discussion at the end of this Section). On the other hand, reduction of the 3<sup>rd</sup> dimension permits to essentially increase the accuracy of the finite-difference time-domain (FDTD) method, used in the COMSOL calculations, due to employment of a finer discrete grid. Therefore, a 2D formulation of the problem allows, in fact, the correct reproduction of the key parameters of the SC-generated output field, while ensuring an optimal balance between calculation accuracy and computational efficiency.

In the scheme of Figure 1, the incident monochromatic plane wave is characterized by the electric field distribution

$$\mathcal{E}^{inc}(y, t) = \text{Re}[\mathbf{E}^{inc}(y)e^{-i\omega t}], \quad \mathbf{E}^{inc}(y) = \mathbf{e}_z E_z^{inc}(y) = \mathbf{e}_z E_0 \exp(-iky) \tag{1}$$

where  $E_z^{inc}$  is the  $z$ -polarized complex amplitude,  $\mathbf{e}_z$  is the  $z$ -directed unit vector,  $k = \omega/c$  is the radiation wavenumber,  $c$  being the velocity of light in vacuum [31]. Accordingly, the scattered field can be expressed as

$$\mathbf{E}(x, y) = \mathbf{e}_z E_z(x, y). \tag{2}$$

Modeling of the interactions induced by the wave (1) in the SC and in the environmental media was performed by the FDTD method, based on the discretization of the Maxwell differential equations. In order to improve the accuracy of calculations, following to works [32, 33], a non-uniform numerical grid with a maximum cell size of  $\lambda/5$  at the dielectric-air interface was used. At the SC-FS and FS-PML boundaries, the standard boundary conditions for the electromagnetic fields were applied; at the external

boundary of PML, the fields are supposed to vanish. Simulations are facilitated by the fact that, like the incident field (1), all the scattered and transformed constituents of the electromagnetic field are  $z$ -polarized, so the whole field existing in the computational domain due to the SC illumination is described by the single  $z$ -component,

$$\mathbf{E}^s(x, y) = \mathbf{e}_z E^s(x, y), \quad E^s(x, y) = E_z^{\text{inc}}(y) + E_z(x, y). \quad (3)$$

It is this field that is the subject of simulations.

Main limitations of the presented 2D consideration are estimated in the [Appendix](#). It shows that the 2D [Equations 1–3](#) produce appropriate results for the middle SC cross section, equally distanced from the SC bases, if the SC length in the  $z$ -direction  $h$  is of the same order of magnitude as  $d$ , or higher. It is this cross section  $z = 0$  that is implied in [Figure 1](#) as well as in all other figures below. Possible corrections include the non-zero longitudinal field components  $E_y^s$ , and the  $z$ -variability of the field components. Associated errors may be most noticeable near the SC surfaces (e.g., at  $z = \pm h/2$ ;  $x, y \sim d/2$ ) but are smoothed with growing off-SC distances. In general, possible relative errors in the field magnitude, associated with the finite SC length, are of the order  $(kh)^{-2}$ , which, upon the usual mesoscale conditions, does not exceed 1% and thus does not impugn the wide validity of the 2D-simulation results presented in this paper.

### 3 Photonic nanojets formed upon excitation by the plane wave with $\lambda = 632.8$ nm

We start with the example where the SC of refractive index  $n_r = 1.46$  (i.e., quartz glass) is illuminated by the plane wave of He-Ne laser radiation,  $\lambda = 632.8$  nm. The general view of the scattered-light distribution obtained in this case is presented in [Figure 2](#); here and in all further figures, the calculated field intensity  $|E^s|^2$  is normalized with respect to the incident-wave intensity  $|E_0|^2$  (see [Equations 1, 3](#)). Additionally, the figures illustrate the distribution of the time-averaged energy flux, calculated as the time-averaged Poynting vector [34].

It is seen that the scattered energy is distributed rather inhomogeneously; regions of the well-expressed energy concentration are formed. In the symmetric case (the SC plane face is orthogonal to the incident wave, [Figure 2b](#)), the picture resembles usual focusing, with the distinction that the light convergence occurs in the near-field zone and with participation of evanescent-field contributions. It represents a classic PNJ involving the whispering-gallery modes [13, 15, 35], and serves here as a base of comparison.

Remarkably, if the SC is situated asymmetrically ([Figure 2a](#)), the scattered-field pattern demonstrates more impressive energy concentration and contains higher number of bright details as compared to the symmetric configuration presented in [Figure 2b](#). That is why the asymmetric situations will be in the focus of our further consideration. Specifically, instead of a single vertical PNJ of [Figure 2b](#), in [Figure 2a](#) several curved strips of high energy concentration cross the bottom boundary of the image approximately at  $x \in (-3, -2)$ ,  $x \in (2.5, 3.1)$ , and  $x \in (3.6, 4.0)$ . Positions, shapes and intensities of such crooked PNJs can be

modified via changing the SC properties and geometry, which opens a potential channel for their control and regulation.

As in conventional PHs [18–23], formation of such complex spatial light patterns, with alternating energy “clots” and “rarefactions”, is caused by the interference of refracted and reflected waves, together with the waveguide and evanescent modes formed by the scattering particle. When an incident plane wave interacts with the convex and flat surfaces of a particle, the optical path lengths in different regions are unequal, leading to phase shifts between the partial waves emerging from different parts of the dielectric SC. As a result of the superposition of these waves in the near field, an oscillatory redistribution of optical intensity is formed on the SC shadow side, manifested as alternating field maxima and minima. In particular, the brightest energy clot of [Figure 2A](#), approaching the bottom boundary at  $x \in (-3, -2)$ , forms a “prototype” of the zigzag-shaped PH.

Further analysis of some specific asymmetric scattering geometries can be performed with the help of [Figure 3](#) where the results of numerical modeling are presented as maps of the field  $|E^s(x, y)/E_0|^2$  for different values of the SC orientation angle  $\alpha$  and diameter  $d$ . It illustrates how the impressive PNJs can be formed at certain combinations of  $d$  and  $\alpha$  ([Figures 3a,b](#)), and how these are gradually transformed into PZ [26] structures ([Figures 3c,d](#)).

Despite the common physical nature with previously reported PH configurations [18–23], the field excited by asymmetric SC shows remarkable distinctions:

1. First to note, the transformed field contains not one but several PNJs of different but comparable intensities and shapes, forming what can be called a “photonic multijet” (PMJ) for convenience (see [Figure 3c](#)).
2. Accordingly, the intensity of a separate PNJ becomes noticeably lower than for the conventional PHs (however, the intensity contrast with the adjacent “dark” regions remains rather high, 3–10 dB).
3. Another distinctive feature is the specific shape of the brightest PNJs, with two or more bends, justifying the “zigzag” name. The “perfect” PZ is well visible in [Figure 3c](#) but the PNJs crossing the bottom border of the images at  $x \approx 2$  in [Figure 3a, b](#) can be considered as “broken” PZs, or not fully formed PZs. It should be noted, however, that, although PZs expose certain specific details of the field configuration, physically these are merely a morphological variation of PHs.
4. This specific morphology is apparently associated with the diffractive origin of the SC-generated PNJs, which causes the root-parabolic trajectory  $y \propto \sqrt{x}$  [20, 36] for relatively large distances (several wavelengths behind the SC), while for conventional PHs the Airy-accelerating behavior  $y \propto x^2$  is more typical [18–23]. Just near the SC output surface, the “Airy-type” behavior prevails but with growing distance of propagation, the root-parabolic law becomes dominant; this reasoning provides a qualitative explanation of the zigzag-like PNJ origin. Additionally, the root-parabolic PNJs’ evolution determines a specific silhouette of the whole SC-produced field pattern, PMJ, which unites these PNJs into a single complex. Its boundaries are approximately depicted by blue dashed lines in [Figure 3c](#).

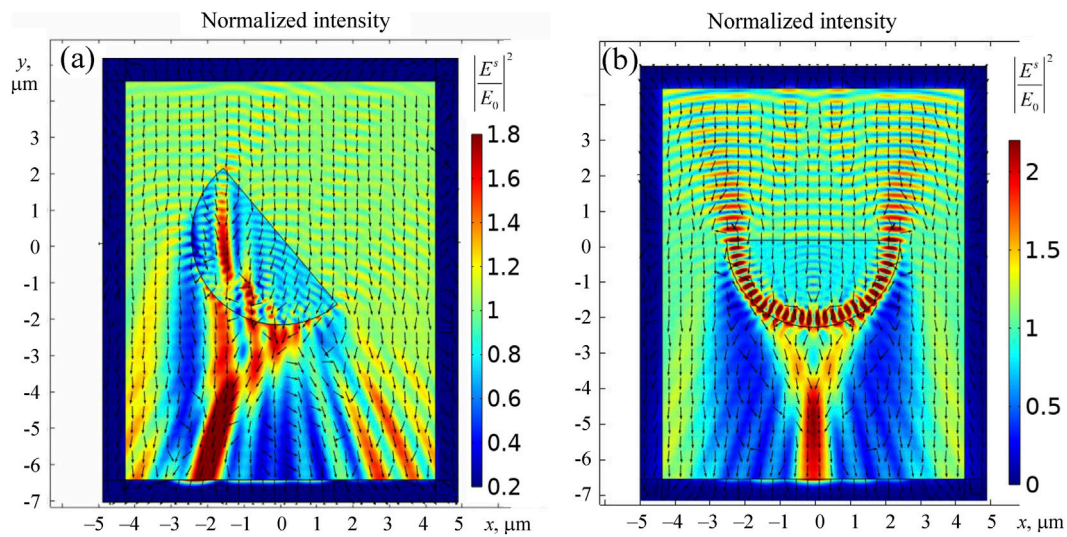


**FIGURE 2** Normalized intensity distribution of the wave with  $\lambda = 632.8$  nm transformed by the SC with  $d = 5$   $\mu\text{m}$ ,  $n_r = 1.46$ . (a) “Geometric-asymmetry” case,  $\alpha = 40^\circ$ ; (b) symmetric case,  $\alpha = 90^\circ$ . The black arrows show directions of the local energy flow density (Poynting vector).

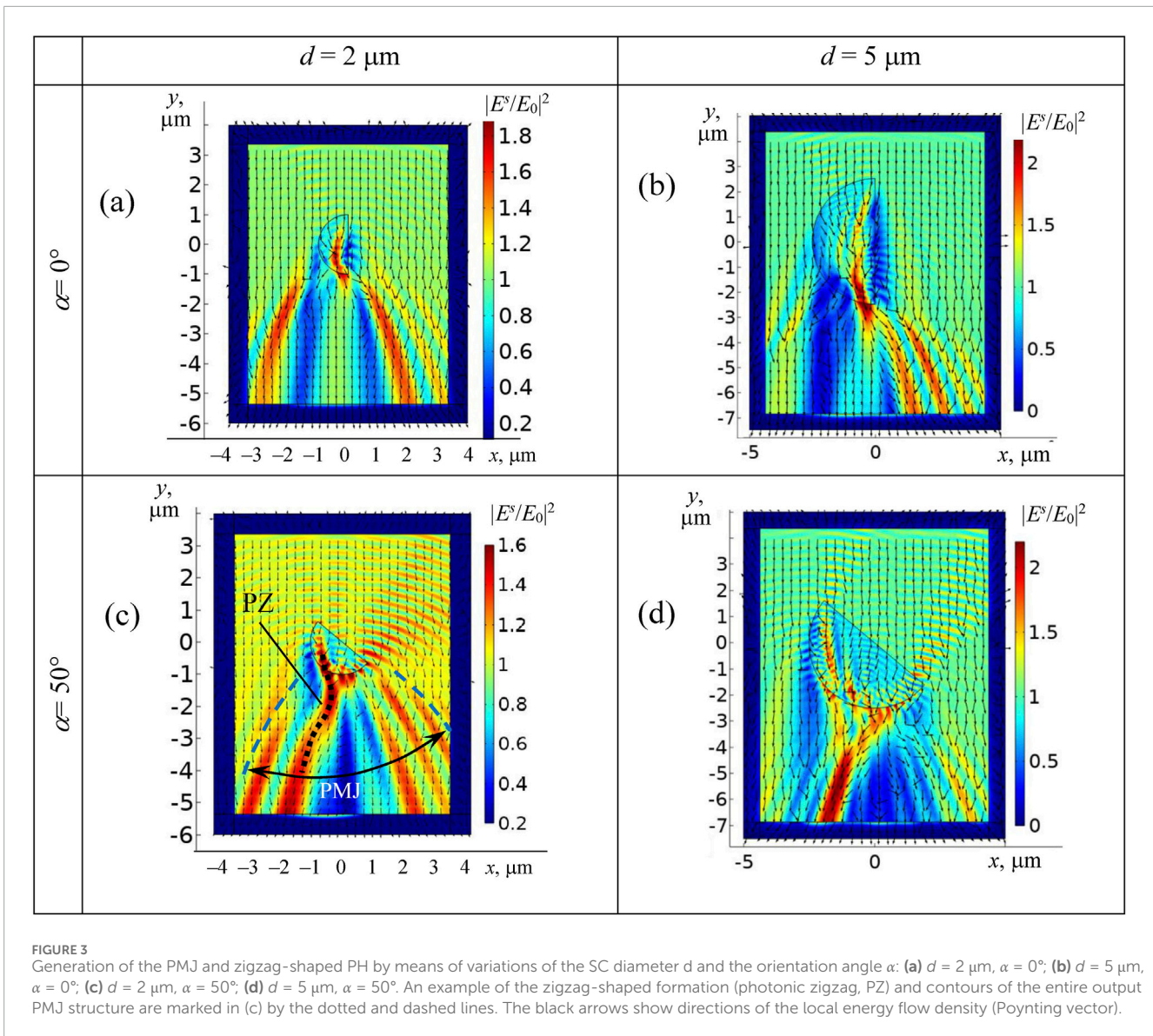
The revealing and characterization of the output-field PMJ structures is, probably, the most remarkable result of the paper. It clearly indicates that an asymmetric SC may act as the source of a coherent set of interrelated PNJs of comparable intensities, whose configurations can be controlled and regulated together and in which the properties of individual PNJs interact and complement each other. Generally speaking, the PMJ is not absolutely new object: Situations of multiple PNJ generation are well known (see, for example, [14, 15, 18, 37–40]) and are employed, e.g., for the formation of arrays of nanoholes and nanopillars in the photoresist layers [40]. But usually such PNJ combinations are formed by rather complex optical constructions based on arrays of identical symmetric microparticles, or phase diffraction gratings [14, 15, 37]. Similar principles govern the formation of special PMJ configurations by composite microparticles of complicated shape, composed of several identical cylinders or spheres (“photonic molecules”) [38]. Situations of PMJ generation by single microparticles of asymmetric shape or under the asymmetric illumination (the most close to the one considered here) were also described [18, 39] but treated as occasional curious facts, without delving into their specific features or methods of control. In this paper, the SC-generated PMJs will be subjects of deeper inspection, with special attention to their controllability, purposeful modification and probable applications.

As usual [12–16, 18–23], a characteristic feature of every PNJ in Figures 2a, 3a–d is the subdiffraction concentration of optical energy. The minimum value of the full width at half-maximum (FWHM) of the PNJ intensity distributions presented in these figures equals to  $\delta \approx 250$  nm, which is below the classical diffraction limit  $\lambda/2$  and is close to the focal-spot sizes available for the conventional PHs [18–23]. For comparison, the Abbe diffraction limit of traditional optical microscopy [34],  $\delta = 0.5\lambda/\text{NA} \approx 348$  nm (for the numerical aperture of the

microscope objective  $\text{NA} \approx 0.9$ ), is also inferior to the degree of light-energy concentration available for PNJs presented in Figures 2, 3.

While the extra-narrow squeezing of optical energy concentration is typical for any PH and symmetric PNJ structures (like that in Figure 2b), the characteristic lateral shifts of the focal maxima, and their trajectories in the  $(x, y)$ -plane appear due to asymmetry of the SC configuration characterized by the orientation angle  $\alpha$ . Figure 3 clearly demonstrates how the shapes of PNJs are influenced by the angle  $\alpha$  and the SC diameter  $d$  (with respect to  $\lambda$ ). A general conclusion can be derived that for a given SC diameter  $d$ , a “perfect” PZ near the vertical axis ( $x = 0$ ) can be obtained at a certain orientation angle  $\alpha$ , accompanied by several “side” root-parabolic PNJs. With deviation from this “perfect-PZ” orientation, the PZ becomes discontinuous, while the side PNJs are spatially shifted and deformed. More specifically, increasing  $d/\lambda$  results in more extended PNJs in the  $y$ -direction (not shown in Figure 3) with gradual shifts of the PNJ trajectories toward the  $y$ -axis (which complies with diffraction-based origins of the PZ structure). The whole PMJ pattern shrinks in the horizontal direction accordingly. Changes of both  $\alpha$  and  $d$  contribute to the energy redistribution between the separate PNJs, preserving the subdiffraction squeezing effect.

These observations underlie the principles of the purposeful PMJ-structure regulation and highlight the potential of asymmetric dielectric-SC scatterers for implementing controllable local displacement and manipulation of light clots in subwavelength photonic systems. For example, existence of several non-overlapping PNJs offers several independent energy-transfer channels. At certain conditions illustrated by Figure 3, two or three of the PNJs are especially bright and can be chosen for specific light splitting and signal branching. In more detail, the backgrounds for possible PMJ applications are discussed in the next Section.



### 4 Potential applications for separation and switching of optical signals

The general ideas, developed in the previous Section based on the modeling results, illustrated in Figures 2, 3, can be applied for creation of the specific tools for separation and switching of optical signals in fiber-optics communication systems and in data-processing technologies.

Due to the dependence of the SC-generated field structure on  $d/\lambda$ , this task can be realized via excitation of the same SC element by incident monochromatic radiation with different wavelengths. As was indicated in the Introduction, there are meaningful reasons to choose  $\lambda_1 = 1310 \text{ nm}$  and  $\lambda_2 = 1550 \text{ nm}$ , and now we proceed to modeling the behavior of SC scatterers of the type, described in Figure 1, under the plane-wave illumination with such wavelengths.

Continuing the consideration of Section 3, we start with the situation where the SC material is fused silica ( $\text{SiO}_2$ ) with the

refractive index  $n_{r1} = 1.447$  (at  $\lambda_1$ ) and  $n_{r2} = 1.444$  (at  $\lambda_2$ ) [41]. As in all other examples, the incident radiation approaches along the  $-y$ -direction (Figure 1). Upon the modeling, values of the SC diameter and orientation angle were variable, and some results are exposed in subsequent figures.

Figures 4a,b shows the intensity maps and Poynting vector distributions for two SC configurations characterized by the same asymmetry (angle  $\alpha$ ) but differing by the SC diameters and radiation wavelengths. However, in the images 4a and 4b the ratio  $d/\lambda \approx 0.846$  is approximately preserved. As can be seen from the figure, the PZ and PNJ shapes for the wavelengths  $\lambda_1$  and  $\lambda_2$  demonstrate high similarity, which confirms the decisive role of the  $d/\lambda$  parameter in their formation. Nevertheless, some differences in fine details of the PNJ configurations may be visible (Figures 4a,b), which can be attributed to the small difference in the refractive indices of the SC material for  $\lambda_1$  and  $\lambda_2$ .

Now consider additional possibilities for the purposeful PMJ-pattern formation, emerging from the variability of the SC material

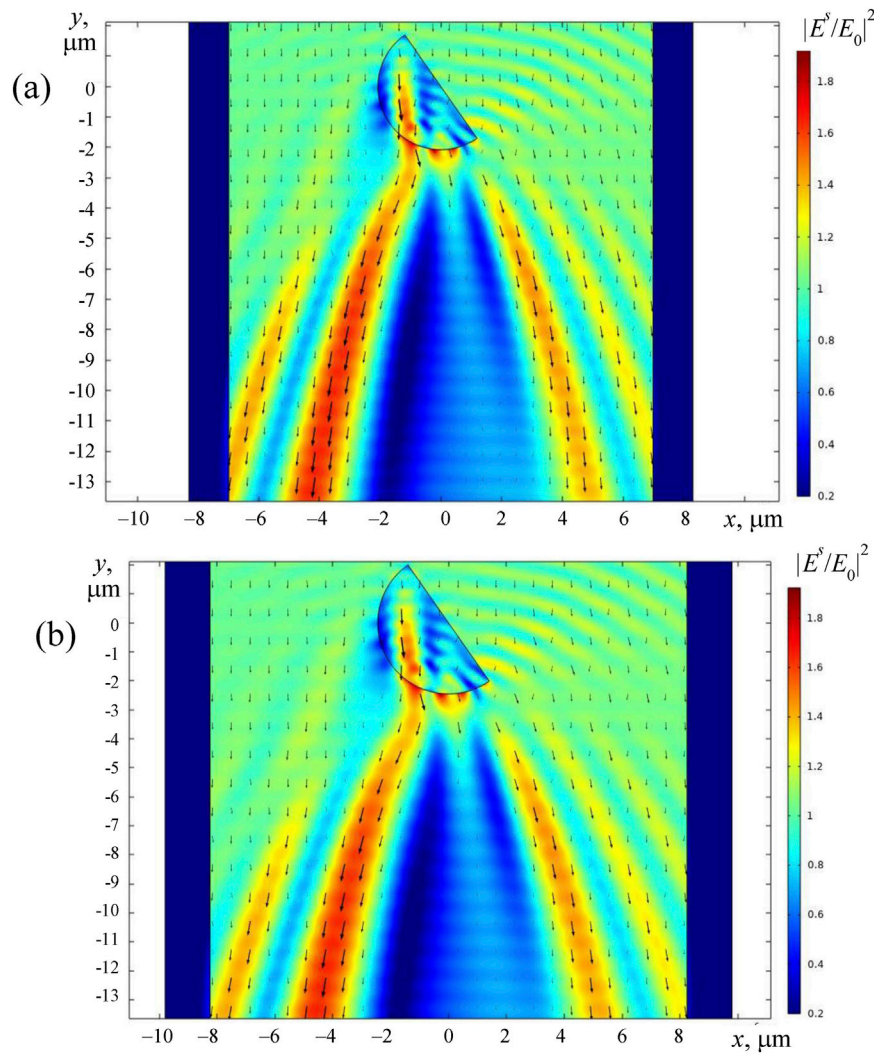


**FIGURE 4** PMJ patterns for wavelengths (a)  $\lambda_1 = 1310$  nm, and (b)  $\lambda_2 = 1550$  nm. The SC material is fused silica; for  $\lambda_1$  (a),  $d_1 = 4.149$   $\mu\text{m}$ ,  $\alpha = 35^\circ$ ; for  $\lambda_2$  (b),  $d_2 = 4.897$   $\mu\text{m}$ ,  $\alpha = 35^\circ$ . The black arrows show the direction and magnitude of the local Poynting vector.

properties. Next figures perform a comparison of the fields excited by the input waves with the wavelengths  $\lambda_1$  and  $\lambda_2$  passing through the SC with the same geometrical and dielectric parameters: in Figure 5,  $d = 7$   $\mu\text{m}$ ,  $\alpha = 20^\circ$ ,  $n_r = 1.7$ , and in Figure 6,  $d = 6$   $\mu\text{m}$ ,  $\alpha = 12^\circ$ ,  $n_r = 1.6$  (such refractive indices are available, for example, for flint-glass or BGG glass [41]). In both cases, a clear spatial separation of the scattered fields formed by the wavelengths  $\lambda_1$  and  $\lambda_2$  can be observed at the SC output.

The image of Figure 5a shows that the PNJs of sufficient intensity with a wavelength of  $\lambda_1 = 1310$  nm cross the bottom boundary at intervals:  $x \in (-8.5, -7.5)$ ,  $x \in (-6.7, -5.8)$ ,  $x \in (2.3, 3.3)$ . On the contrary, the PNJs of  $\lambda_2 = 1550$  nm (Figure 5b) cross the bottom boundary at intervals  $x \in (-8.0, -6.8)$ ,  $x \in (3.7, 4.5)$ ,  $x \in (6.0, 7.0)$ . Only at negative  $x$  these intervals partly overlap; therefore, in the  $x > 0$  region, the PNJs of different wavelengths do not intersect in the space. Likewise, in Figure 6a the four PNJs with a wavelength of  $\lambda_1 = 1310$  nm cross the lower boundary of the figure at intervals  $x \in (-8.25, -7.85)$ ,  $x \in (-6.6, -5.3)$ ,  $x \in (2.15,$

$3.0)$ ,  $x \in (4.55, 5.0)$ , and in Figure 6b, the four PNJs with  $\lambda_2 = 1550$  nm cross the bottom border at intervals  $x \in (-7.85, -6.6)$ ,  $x \in (1.0, 2.0)$ ,  $x \in (3.75, 4.75)$ ,  $x \in (6.25, 7.25)$ . All these intervals practically do not overlap, and the corresponding PNJs for  $\lambda_1$  and  $\lambda_2$  are spatially separated. Accordingly, the micro-receivers properly placed at the corresponding areas (for example, PIN photodiodes with the input window size  $< 3$   $\mu\text{m}$  [42, 43] and/or equipped by the appropriate field diaphragm) will allow for separate registering the signals with wavelengths  $\lambda_1$  and  $\lambda_2$ . This means that the SCs of the types presented in Figures 5, 6 can act as wavelength splitters that can be implemented in photonic microcircuits.

Another interesting version of the PMJ structure is realized at the output of a fused-silica SC with parameters  $d = 4$   $\mu\text{m}$ ,  $\alpha = 25^\circ$  (Figure 7). In this case,  $n_{r1} = 1.447$  (at  $\lambda_1 = 1310$  nm, Figure 7a) and  $n_{r2} = 1.444$  (at  $\lambda_2 = 1550$  nm, Figure 7b). The PNJs with wavelength  $\lambda_1$  cross the bottom boundary of Figure 7a at intervals  $x \in (-6.0, -5.0)$ ,  $x \in (-3.8, -2.7)$ ,  $x \in (2.8, 3.8)$ ,  $x \in (5.2, 5.8)$ , and those with  $\lambda_2 = 1550$  nm cross the bottom boundary of Figure 7b at intervals

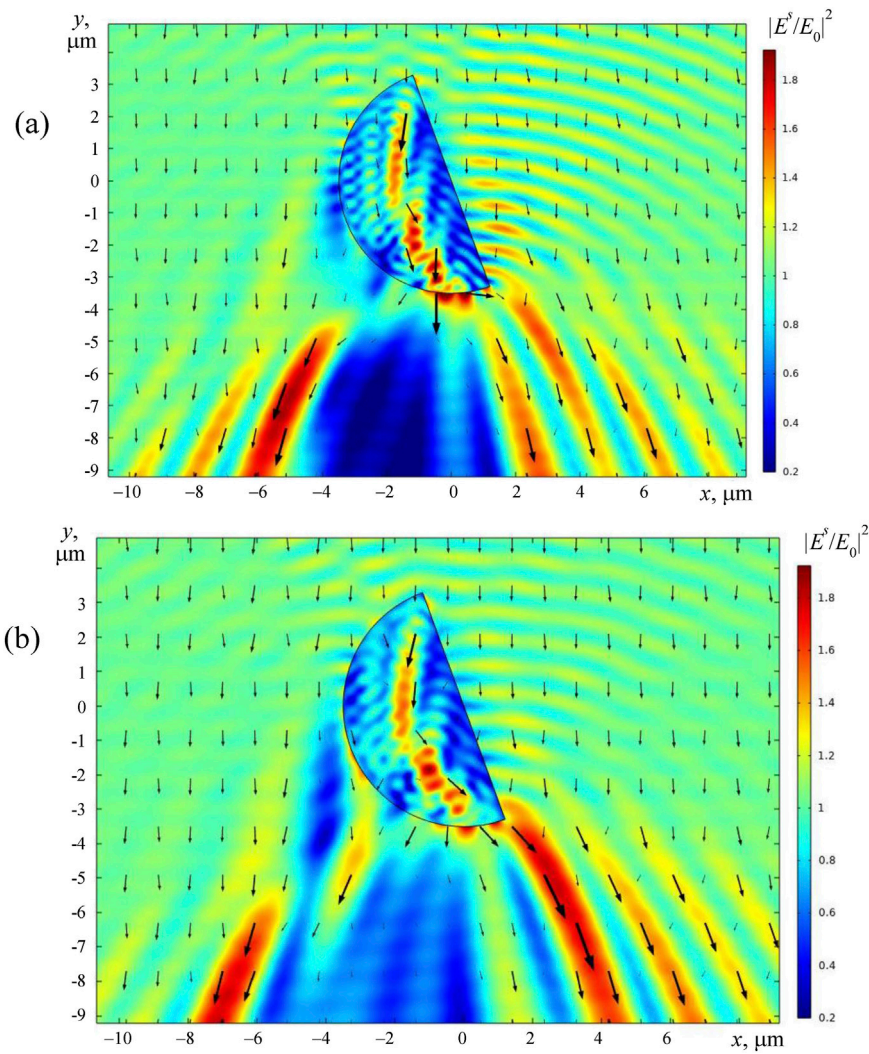


**FIGURE 5** Views of the PMJ patterns excited by the incident plane waves with wavelengths (a)  $\lambda_1 = 1310$  nm and (b)  $\lambda_2 = 1550$  nm. The SC parameters in (a) and (b) are identical and equal to:  $d = 7 \mu\text{m}$ ,  $\alpha = 20^\circ$ ,  $n_r = 1.7$ . The black arrows show the direction and magnitude of the local energy flow density (Poynting vector).

$x \in (-4.4, -2.8)$ ,  $x \in (1.0, 2.2)$ ,  $x \in (3.8, 4.7)$ ,  $x \in (6.0, 6.75)$ . Like in cases of Figures 5, 6, most of these intervals do not overlap. However, contrary to Figures 5, 6, the interval  $x \in (-3.8, -2.7)$  of Figure 7a essentially overlaps the interval  $x \in (-4.4, -2.8)$  of Figure 7b. Thus, we can conclude that a sort of spatially distributed sensor selectivity can be realized: Signals of different wavelengths can be registered separately by micro-receivers placed in the region  $x > 0$ , while the combined signal uniting the contributions of  $\lambda_1$  and  $\lambda_2$  can be “captured” by an entrance window positioned, e.g., at  $x \in (-4, -2.8)$ , and transmitted to further circuit elements.

The series of examples can be continued but the results already obtained are sufficient to indicate certain expected applications of the switching elements based on the SC with geometric asymmetry, considered in this paper. At present, two modes of operation can be envisaged. The first one is the switching mode, where the SC scatterer acts as a passive switching element capable of dynamically altering the electromagnetic field distribution depending on the spectral

conditions of the external irradiation (1310 nm or 1550 nm), opening up potential applications in nanophotonic systems for controlled signal modulation. The second one is the splitting mode, where the two signals propagate together (e.g., along a single-mode optical fiber) and are then precisely separated. Consequently, the generated optical signals can be switched to prescribed routes based on the PNJs’ trajectories of the PMJs. Existence of several PNJs in the field formed by an asymmetric SC provides a theoretical possibility of combining several functionalities in a single SC-based mesoscale optical element.

The analysis of a specific operating switching system is not a goal of this paper but the numerical simulation enabled us to estimate some relevant parameters:

1. The expected energy losses of switched signals are significant, 65%–80%, i.e., they require the use of a quantum signal amplifier. Such a high level of losses is explained by the two main reasons:

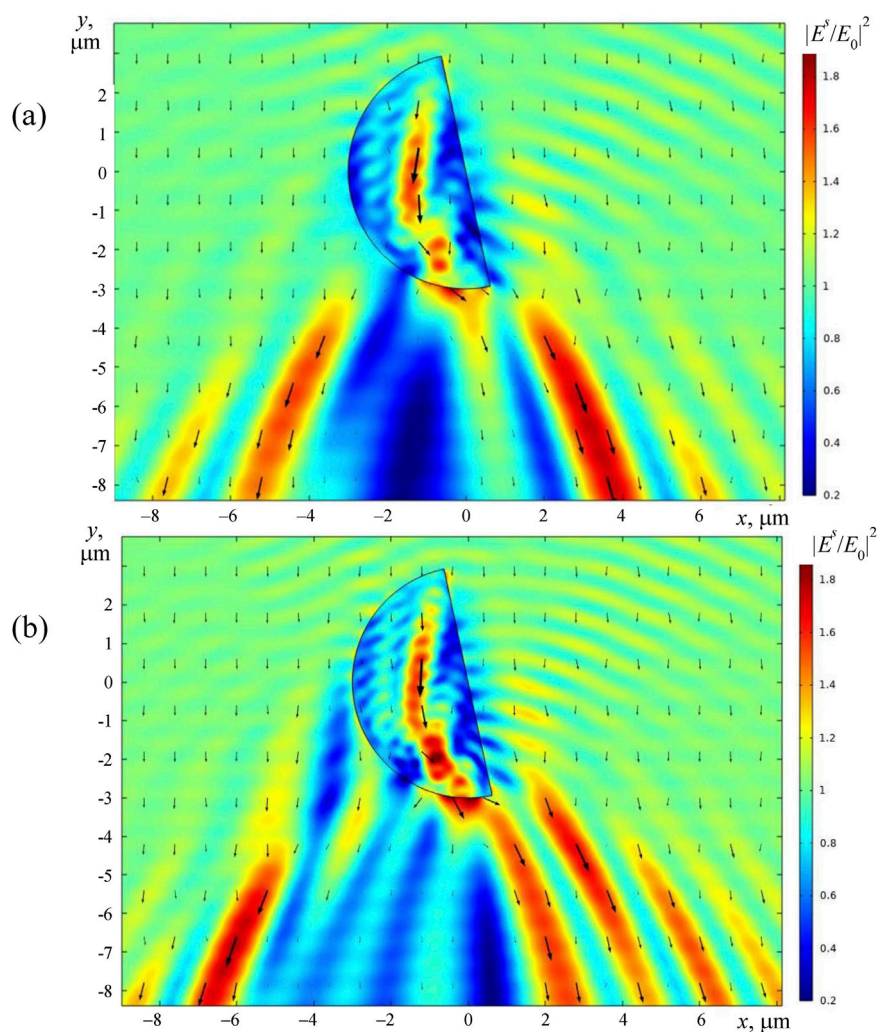


**FIGURE 6**

Views of the PMJ patterns excited by the incident plane waves with wavelengths (a)  $\lambda_1 = 1310$  nm and (b)  $\lambda_2 = 1550$  nm. The SC parameters in (a) and (b) are identical and equal to:  $d = 6$   $\mu\text{m}$ ,  $\alpha = 12^\circ$ ,  $n_r = 1.6$ . The black arrows show the direction and magnitude of the local energy flow density (Poynting vector).

inevitable division of the field energy between several channels, some of which take no part in the energy transfer, and the 2D character of individual PNJs, due to which the energy only concentrates in the transverse cross section ( $x, y$ ) but still scatters along the  $z$ -axis (see Figure 1). In the prospective applications, the second effect may probably be removed or weakened, e.g., via additional focusing along the  $z$ -axis.

2. The negative expectation of high losses is partly balanced by low dimensions of the anticipated optical switch: these can be significantly smaller than the dimensions of systems with dichroic filters, diffraction gratings or dispersion prisms and can be encapsulated in a fiber-optic cable.
3. Spectral mixing of channels is at least 15 dB when using a 1  $\mu\text{m}$  slit in front of the signal receiver (photodiode or optical-fiber input window).

The latter indicator is not very favorable. Even reducing the slit width to 0.75  $\mu\text{m}$  enables a spectral-noise decrease up to 25 dB,

which is worse in comparison with wavelength dividers based on dichroic elements, where the separation reaches 30 dB. But the undoubted advantage of the proposed PMJ-based approach is the possibility of creating devices with much smaller dimensions. Anyway, the detailed analysis of its possible applications and specific device configurations should be the subject of a special work.

To finalize the discussion on practical implementation of the above-described PMJ principles, we briefly touch the problem of suitable and reliable manufacturing of high-quality transparent SCs with a diameter of 2–5  $\mu\text{m}$ . A detailed investigation of this problem is, again, beyond the scope of the paper but we can mention some promising principles of the expected technologies.

Traditional methods of processing glass and other materials (grinding, polishing) are not suitable for such miniature sizes and complex shapes. However, there are several new methods for the SC manufacturing. In the microlens laser marking method [44], a laser beam is focused and modifies a material according to a pre-designed 3D pattern. The final SC structure is then formed using

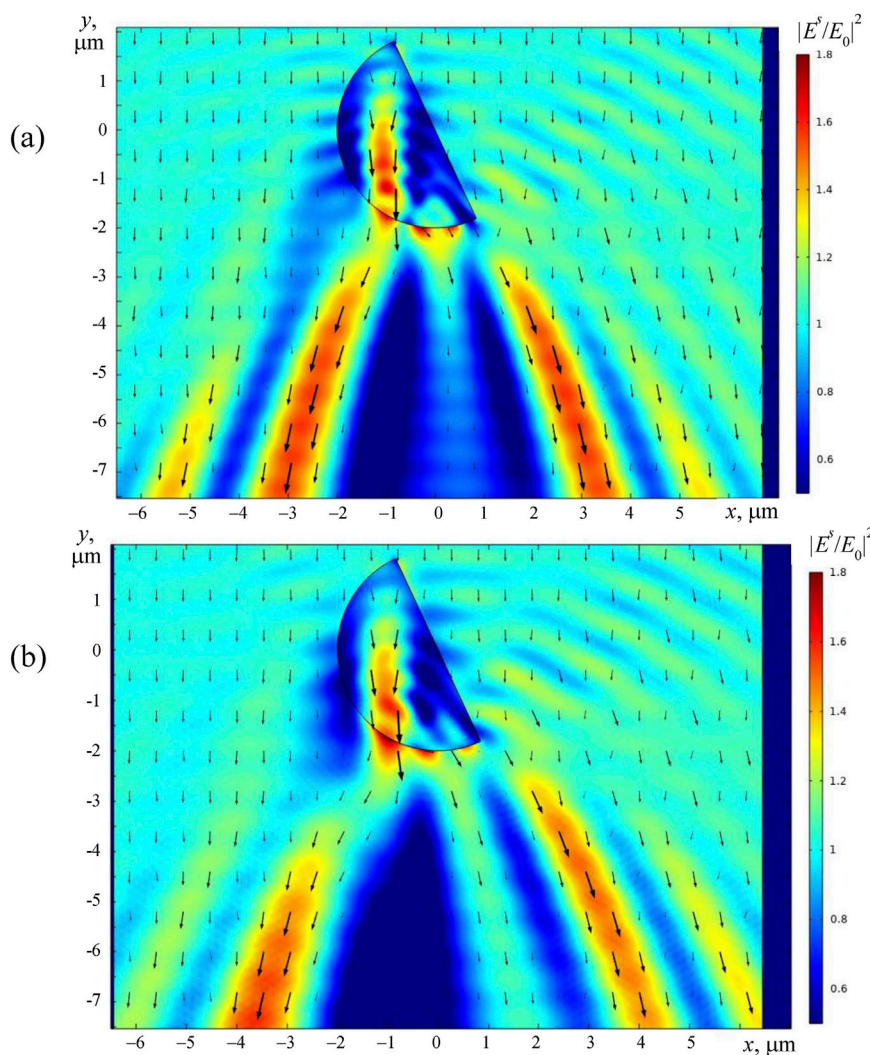


**FIGURE 7**

Views of the PMJs excited by the incident plane waves with wavelengths (a)  $\lambda_1 = 1310$  nm and (b)  $\lambda_2 = 1550$  nm. The SC material is fused silica, its geometric parameters in (a) and (b) are identical and equal to:  $d = 4$   $\mu\text{m}$ ,  $\alpha = 25^\circ$ . The black arrows show the direction and magnitude of the local energy flow density (Poynting vector).

etching or plasma polishing. A much more accurate method uses a photoresist or electron beam resist, which is applied onto the source material, exposed, and developed [45]. Typically, the SC is fabricated as an element of a microlens array on a substrate, rather than as a separate element [46].

To create a SC of the required size on the base material, deep reactive ion etching (DRIE) with a plasma containing inert or reactive gases (e.g.,  $\text{CF}_4$ ,  $\text{C}_4\text{F}_8$ , or  $\text{SF}_6$ ) can be used [47]. To improve the optical quality and reduce surface roughness, thermal smoothing (post-etch annealing) can be applied: the etched structure is subjected to high-temperature (over 1000  $^\circ\text{C}$ ) annealing [48]. At this temperature, surface tension can smooth out etching-induced micro-irregularities, making the surface more optically clean and smooth, which is critical for a high-quality mesoscale element. Another, much more precise method of reducing surface roughness is  $\text{CO}_2$  laser polishing (Laser Smoothing) [49]. The final SC quality is assessed by two main parameters: accuracy of its dimensions

and accuracy of its profile, using the scanning electron microscopy (SEM) or atomic force microscopy (AFM) [50]. Its optical validity is limited by the surface roughness, which should not exceed a few nanometers [51].

An alternative approach to the SC fabrication, which may be essentially simpler upon the laboratory conditions, can be realized on the ground of the optical-fiber manufacturing technologies, which are now well developed [52]. Normally, these enable to produce a high-quality optical fiber of the required diameter and refractive index. At the next stage, the fiber segments are glued to a high-quality strictly-flat substrate and polished to half the diameter. All assembly operations can be carried out under a microscope using a micromanipulator; the microcylinder orientation is carried out with the help of a microgoniometer (generally applied for orientation of crystals).

This combination of technologies opens the possibility for creating complex photonic structures of arbitrary geometry with

high optical surface quality and controlled refractive parameters. All this may be applied for fabrication of the photonic splitter developed in this paper, which thus will combine compactness, technological compatibility with existing optical platforms, and scalability, making it promising for the use in nanophotonics, sensor systems, and next-generation optical communications.

## 5 Conclusion

This paper presents the results of computer simulation of the plane-wave scattering on a mesoscale dielectric semicylinder (SC). It was revealed that the transformed field pattern presents highly inhomogeneous structured-light distribution, with possible concentration of the light energy within several strictly localized trajectories (photonic nanojets–PNJs) [9–16]. These PNJs, generally, possess curvilinear shapes thus belonging to the family of photonic hooks (PHs) [18–23], and all together form the so called “photonic multijet” (PMJ). The observed scattering-field patterns (number and intensities of separate PNJs, their spatial positions, shapes and orientations) depend on the SC dielectric parameters, its size (relative to the incident radiation wavelength), and its orientation with respect to the incident wave. The most interesting behavior appears when the SC plane face is oriented at a certain angle (different from 0° to 90°) with respect to the incident light direction (“geometric asymmetry” condition). Accordingly, several configurations with the geometric asymmetry were considered in more detail.

The modeling results testify for the productivity of the PMJ concept: the asymmetric-SC-generated field can be considered as a single complex, in which the separate PNJs evolve coherently, interacting and complementing each other. The configuration and intensity characteristics of the PMJ field depend on the incident-light wavelength and the SC geometry, which opens ways for its deliberate modifications and control. Accordingly, our results show that the SC-generated fields (PMJs) and their structure elements (PNJs) can be employed for creation of controllable photonic switches and splitters for optical signal processing, data storage and transformation. The envisaged photonic splitters may be useful for controlling the directions of predominant light propagation (output channels), their efficiencies (intensity distribution between the different PNJs) and spatial localization. The simulation results determine the key optical parameters and optimized geometric characteristics of the proposed switching elements, indicate ways for their control and regulation, as well as prospects for their experimental implementation, which is important for the construction of integrated nanophotonic circuits.

A distinctive feature of the proposed splitter design is the possibility of efficient separation of monochromatic light components with two specified wavelengths ( $\lambda_1 = 1310$  nm and  $\lambda_2 = 1550$  nm). Peculiar features of the scattered fields formed by the separate spectral components enable the creation of spectral-sensitive photonic switches, spectral routers, etc., compatible with the existing telecommunications infrastructure. The detailed analysis of a specific operating switching system is beyond the scope of the present paper and should be a subject of a separate work, but some relevant estimations made in Section 4 indicate that the SC-generated PMJ structures may be considered as a prototype of efficient and practically suitable photonic devices. The results of PMJ modeling open the way

to the implementation of SC-based microscale photonic switches and spectral routers that can be built into integrated photonic circuits without the need for additional components.

Finally, it is reasonable to mention some limitations of the proposed approach and plausible prospects of its further development. Probably, the main limitations originate from simplifications inherent in 2D consideration accepted in this paper. This issue is considered in Appendix and in the final paragraph of Section 2 where it is shown that, despite the possible distortions at localized spatial regions near the SC surface, it gives appropriate results for the general PMJ field configuration and the individual PNJs’ morphologies in the plane  $z = 0$  corresponding to the middle SC section, provided that the SC end faces (bases) are separated from this plane by the distance  $\geq \lambda$ .

On the other hand, restriction to the plane-wave exciting light, polarized strictly along the SC axis, leaves aside many attractive incident-wave configurations and associated influences on the scattered-field behavior. Expectedly, interesting modifications of the scattered field may be observed if the incident light possess additional structural properties, e.g., circular polarization, phase/polarization singularities, or orbital angular momentum [31, 53–59]. We hope that such modifications will be subjects of further studies, which, however, are beyond the scope of the present work.

## Data availability statement

The raw data supporting the conclusions of this article will be made available by the authors, without undue reservation.

## Author contributions

OA: Methodology, Supervision, Writing – original draft, Writing – review and editing. AB: Conceptualization, Supervision, Writing – original draft, Writing – review and editing. CZ: Conceptualization, Formal Analysis, Validation, Writing – original draft, Writing – review and editing. MG: Methodology, Software, Visualization, Writing – original draft, Writing – review and editing. PM: Conceptualization, Investigation, Methodology, Project administration, Writing – original draft, Writing – review and editing. OM: Data curation, Investigation, Software, Validation, Writing – original draft, Writing – review and editing. SS: Formal Analysis, Investigation, Methodology, Resources, Writing – original draft, Writing – review and editing. JZ: Funding acquisition, Project administration, Resources, Supervision, Writing – original draft, Writing – review and editing. JC: Data curation, Funding acquisition, Supervision, Validation, Writing – original draft, Writing – review and editing.

## Funding

The author(s) declared that financial support was received for this work and/or its publication. Research Institute of Zhejiang University—Taizhou, Center for Modern Optical Technology, China; National Research Foundation of Ukraine (NRFU), project No 2025.07/0069 “Recent applications of structured optical fields

in polarization-interference methods for solving problems in telecommunication and biomedicine”.

## Conflict of interest

The author(s) declared that this work was conducted in the absence of any commercial or financial relationships that could be construed as a potential conflict of interest.

## Generative AI statement

The author(s) declared that generative AI was not used in the creation of this manuscript.

## References

- Baranov D, Zuev D, Lepeshov S, Kotov O, Krasnok A, Evlyukhin A. All-dielectric nanophotonics: the quest for better materials and fabrication techniques. *Optica* (2017) 4:814–25. doi:10.1364/OPTICA.4.000814
- Maier SA. *Plasmonics: fundamentals and applications*. Springer (2007).
- Stockman MI. Nanoplasmonics: past, present, and glimpse into future. *Opt Express* (2011) 19(22):22029–106. doi:10.1364/OE.19.022029
- Kuznetsov AI, Miroshnichenko AE, Brongersma ML, Kivshar YS, Luk'yanchuk B. Optically resonant dielectric nanostructures. *Science* (2016) 354(6314):aag2472. doi:10.1126/science.aag2472
- Jahani S, Jacob Z. All-dielectric metamaterials. *Nat Nanotechnology* (2016) 11:23–36. doi:10.1038/nnano.2015.304
- Staude I, Schilling J. Metamaterial-inspired silicon nanophotonics. *Nat Photon* (2017) 11:274–84. doi:10.1038/nphoton.2017.39
- Minin OV, Minin IV. Optical phenomena in mesoscale dielectric particles. *Photonics* (2021) 8(12):591. doi:10.3390/photronics8120591
- Minin IV, Minin OV. Optical phenomena in mesoscale dielectric three- and two-dimensional structures. (2021):06219. arXiv:2111.1048550/arXiv.2111.06219.
- Heifetz A, Kong S-C, Sahakian AV, Taflove A, Backman V. Photonic nanojets. *J Comput Theor Nanosci* (2009) 6(9):1979–92. doi:10.1166/jctn.2009.1254
- Ferrand P, Wenger J, Devilez A, Pianta M, Stout B, Bonod N. Direct imaging of photonic nanojets. *Opt Express* (2008) 16:6930–40. doi:10.1364/OE.16.006930
- Sharapova PR, Kruk SS, Soltsev AS. Nonlinear dielectric nanoresonators and metasurfaces: toward efficient generation of entangled photons. *Laser & Photon Rev* (2023) 17(4):2200408. doi:10.1002/lpor.202200408
- Kim MS, Scharf T, Mühlhig S, Rockstuhl C, Herzig HP. Engineering photonic nanojets. *Opt Express* (2011) 19(11):10206–20. doi:10.1364/OE.19.010206
- Luk'yanchuk B, Paniagua-Domínguez R, Minin I, Minin O, Wang Z. Refractive index less than two: photonic nanojets yesterday, today and tomorrow. *Opt Mater Express* (2017) 7(6):1820–47. doi:10.1364/OME.7.001820
- Minin IV, Liu C-Y, Geints YE, Minin OV. Recent advances in integrated photonic jet-based photonics. *Photonics* (2020) 7(2):41. doi:10.3390/photronics7020041
- Darafsheh A. Photonic nanojets and their applications. *J Phys Photon* (2021) 3:022001. doi:10.1088/2515-7647/abdb05
- Wang Z, Luk'yanchuk B, Minin IV. Special issue on photonic jet: science and application. *Photonics* 9. Basel, Switzerland: MDPI (2022). p. 540. doi:10.3390/photronics9080540
- Lewis RV. Spider silk: ancient ideas for new biomaterials. *Chem Rev* (2006) 106(9):3762–74. doi:10.1021/cr010194g
- Yue L, Minin OV, Wang Z, Monks JN, Shalin AS, Minin IV. Photonic hook: a new curved light beam. *Opt Lett* (2025) 43(4):771–4. doi:10.1364/OL.43.000771
- Minin IV, Minin OV, Katyba GM, Chernomyrdin NV, Kurlov VN, Zaytsev KI. Experimental observation of a photonic hook. *Appl Phys Lett* (2019) 114(3):031105. doi:10.1063/1.5065899
- Minin IV, Minin OV, Yue L, Wang Z, Volkov VS, Christodoulides DN. Photonic hook – a new type of subwavelength self-bending structured light beams: a tutorial review. (2019):09543. arXiv:1910.1048550/arXiv.1910.09543.
- Dholakia K, Bruce GD. Optical hooks. *Nat Photon* (2019) 13:229–30. doi:10.1038/s41566-019-0403-9
- Tang F, Shang Q, Yang S, Wang T, Melinte S, Zuo C. Generation of photonic hooks from patchy microcylinders. *Photonics* (2021) 8:466. doi:10.3390/photronics8110466
- Dinh Q-T, Wu Y-C, Chen W-Y, Chen Y-B, Minin OV, Minin IV. Photonic hook shaping achieved by the micro-nano fiber array based janus cylindrical metalens. *Phys Scr* (2024) 99:125553. doi:10.1088/1402-4896/ad9119
- Siviloglou GA, Christodoulides DN. Accelerating finite energy airy beams. *Opt Lett* (2007) 32:979–81. doi:10.1364/ol.32.000979
- Chen Z, Taflove A, Backman V. Photonic nanojet enhancement of backscattering of light by nanoparticles. *Opt Express* (2004) 12(7):1214–20. doi:10.1364/OPEX.12.001214
- Gavryliak MS, Maksimyak AP, Maksimyak PP. Formation a photonic zigzag by a half cylinder. *Proc SPIE* (2021):12126. doi:10.1117/12.2615193
- Kong SC, Sahakian A, Taflove A, Backman V. Photonic nanojet-enabled optical data storage. *Opt Express* (2008) 16(18):13713–9. doi:10.1364/OE.16.013713
- Yue L, Wang Z, Yan B, Xie Y, Geints YE, Minin OV. Near-field light-bending photonic switch: physics of switching based on three-dimensional poynting vector analysis. *Photonics* (2022) 9:154. doi:10.3390/photronics9030154
- Pryor RW. *Multiphysics modeling using COMSOL®: a first principles approach*. Sudbury, Massachusetts: Jones & Bartlett Publishers (2009).
- Werner DH, Raj M. A systematic study of perfectly matched absorbers. In: *Frontiers in electromagnetics*. Piscataway, NJ, USA: IEEE Press (2000). p. 609–43. doi:10.1109/9780470544686.ch14
- Bekshaev AY, Bliokh KY, Soskin MS. Internal flows and energy circulation in light beams. *J Opt* (2011) 13(5):053001. doi:10.1088/2040-8978/13/5/053001
- Yi KJ, Wang H, Lu YF, Yang ZY. Enhanced raman scattering by self-assembled silica spherical microparticles. *J Appl Phys* (2007) 101(6):063528. doi:10.1063/1.2450671
- Holms K, Hourahine B, Papoff F. Calculation of internal and scattered fields of axisymmetric nanoparticles at any point in space. *J Opt A: Pure Appl Opt* (2009) 11(5):054009. doi:10.1088/1464-4258/11/5/054009
- Born M, Wolf E. *Principles of optics: electromagnetic theory of propagation, interference and diffraction of light*. Elsevier (2013).
- Zhou S, Deng Y, Zhou W, Yu M, Urbach HP, Wu Y. Effects of whispering gallery mode in microsphere super-resolution imaging. *Appl Phys B* (2017) 123:236. doi:10.1007/s00340-017-6815-7
- Wei P-K, Chou H-L, Chang W-L. Diffraction-induced near-field optical images in mesoscale air-dielectric structures. *J Opt Soc Am B* (2003) 20(7):1503–7. doi:10.1364/josab.20.001503
- Sun Z, Ge S, Shen L, Li J, Xu S, Zhang J. Geometry-dependent photonic nanojet formation and arrays coupling. *Nanomaterials* (2026) 16(2):136. doi:10.3390/nano16020136
- Gerlach M, Rakovich YP, Donegan JF. Nanojets and directional emission in symmetric photonic molecules. *Opt Express* (2007) 15(25):17343–50. doi:10.1364/OE.15.017343
- Rezaei B, Yahyapour B, Darafsheh A. Terahertz tunable three-dimensional photonic jets. *Scientific Rep* (2024) 14(1):16522. doi:10.1038/s41598-024-64158-6

Any alternative text (alt text) provided alongside figures in this article has been generated by Frontiers with the support of artificial intelligence and reasonable efforts have been made to ensure accuracy, including review by the authors wherever possible. If you identify any issues, please contact us.

## Publisher's note

All claims expressed in this article are solely those of the authors and do not necessarily represent those of their affiliated organizations, or those of the publisher, the editors and the reviewers. Any product that may be evaluated in this article, or claim that may be made by its manufacturer, is not guaranteed or endorsed by the publisher.

40. Wu W, Katsnelson A, Memis OG, Mohseni H. A deep sub-wavelength process for the formation of highly uniform arrays of nanoholes and nanopillars. *Nanotechnology* (2007) 18:485302. doi:10.1088/0957-4484/18/48/485302
41. Refractive. Refractive index info. (2025). Available online at: [https://refractiveindex.info/?shelf=glass&book=fused\\_silica&page=Malitson](https://refractiveindex.info/?shelf=glass&book=fused_silica&page=Malitson) (Accessed November 9, 2025).
42. Paschotta R. P-i-n photodiodes. In: *RP photonics encyclopedia* (2025). Available online at: [https://www.rp-photonics.com/p\\_i\\_n\\_photodiodes.html](https://www.rp-photonics.com/p_i_n_photodiodes.html) (Accessed November 4, 2025).
43. Beling A, Campbell JC. High-speed photodiodes. *IEEE J Selected Top Quan Electronics* (2014) 20(6):57–63. doi:10.1109/JSTQE.2014.2341573
44. Yan B, Yue L, Monks JN, Yang X, Xiong D, Jiang C. Superlensing plano-convex-microsphere (PCM) lens for direct laser nano marking and beyond. *Opt Lett* (2020) 45:1168–71. doi:10.1364/OL.380574
45. Cui Z, Du J, Guo Y. Overview of grey-scale photolithography for micro-optical elements fabrication. *Proc SPIE* (2003) 4984:111–7. doi:10.1117/12.477831
46. Popovic Z, Sprague RA, Neville Connell GA. Technique for monolithic fabrication of microlens arrays. *Appl Opt* (1988) 27(7):1281–4. doi:10.1364/AO.27.001281
47. Ouyang Z, Ruzic DN, Kiehlbauch M, Schrinisky A, Torek K. Etching mechanism of the single-step through-silicon-via dry etch using SF<sub>6</sub>/C<sub>4</sub>F<sub>8</sub> chemistry. *J Vac Sci Technol* (2014) 32(4):041306. doi:10.1116/1.4885500
48. Kolari K, Vehmas T, Svensk O, Törmä P, Aalto T. Smoothing of microfabricated silicon features by thermal annealing in reducing or inert atmospheres. *Phys Scr* (2010) T141:014017. doi:10.1088/0031-8949/2010/T141/014017
49. Mendez E, Nowak KM, Baker HJ, Villarreal FJ, Hall DR. Localized CO<sub>2</sub> laser damage repair of fused silica optics. *Appl Opt* (2006) 45(21):5358–67. doi:10.1364/AO.45.005358
50. Delvallée A, Feltn N, Ducourtieux S, Trabelsi M. Comparison of nanoparticle diameter measurements by atomic force microscopy and scanning electron microscopy. In: *16th international congress of metrology 06007*. Les Ulis, France: EDP Sciences (2013). doi:10.1051/metrology/201306007
51. Yuan W, Li LH, Lee WB, Chan CY. Fabrication of microlens array and its application: a review. *Chin J Mech Eng* (2018) 31(1):16. doi:10.1186/s10033-018-0204-y
52. Kaminow I, Li T *Optical fiber telecommunications IV-B: systems and impairments* 2. Elsevier (2002).
53. Dennis MR, O'Holleran K, Padgett MJ. Singular optics: optical vortices and polarization singularities. *Prog Opt* (2009) 53:293–363. doi:10.1016/S0079-6638(08)00205-9
54. Zhao Y, Edgar JS, Jeffries GD, McGloin D, Chiu DT. Spin-to-orbital angular momentum conversion in a strongly focused optical beam. *Phys Rev Lett* (2007) 99(7):073901. doi:10.1103/PhysRevLett.99.073901
55. Bekshaev A. A simple analytical model of the angular momentum transformation in strongly focused light beams. *Cent Eur J Phys* (2010) 8(6):947–60. doi:10.2478/s11534-010-0011-2
56. Gbur G. Singular optics. In: *The optics encyclopedia*. Wiley Online Library (2015). p. 1–23. doi:10.1002/9783527600441.oe1011
57. Angelsky OV, Bekshaev AY, Mokhun II, Vasnetsov MV, Zenkova CY, Hanson SG. Review on the structured light properties: rotational features and singularities. *Opto-electronics Rev* (2022) 30(2):e140860. doi:10.24425/opele.2022.140860
58. Angelsky OV, Bekshaev AY, Vasnetsov MV, Zenkova CY, Maksimyak PP, Zheng J. Optical phase singularities: physical nature, manifestations and applications. *Front Phys* (2022) 10:1060787. doi:10.3389/fphy.2022.1060787
59. Angelsky OV, Mokhun II, Bekshaev AY, Zenkova CY, Zheng J. Polarization singularities: topological and dynamical aspects. *Front Phys* (2023) 11:1147788. doi:10.3389/fphy.2023.1147788

## Appendix: Validation of the 2D model

Maxwell equations for the harmonic light fields oscillating with frequency  $\omega$  in a non-magnetic dielectric medium with permittivity  $\epsilon$  can be written in the form [34]

$$\nabla \times \mathbf{E}^s = ik\mathbf{H}^s, \quad \nabla \times \mathbf{H}^s = -ik\epsilon\mathbf{E}^s, \quad \nabla \cdot \mathbf{H}^s = 0, \quad \nabla \cdot (\epsilon\mathbf{E}^s) = 0. \quad (\text{A1})$$

where  $\mathbf{E}^s$ ,  $\mathbf{H}^s$  are the complex-valued time-independent phasors introduced like  $\mathbf{E}^{inc}$  in Equation 1. From Equation A1, the equation for the electric field immediately follows:

$$\nabla^2 \mathbf{E}^s + k^2 \epsilon \mathbf{E}^s = \nabla(\nabla \cdot \mathbf{E}^s). \quad (\text{A2})$$

Under the usual conditions where the medium is homogeneous, the r.h.s of (A2) vanishes, and it reduces to the Helmholtz equation. Now consider application of Equation A2 to the problem of Figure 1, and recast it using the Cartesian components of the electric field. For simplicity, we suppose  $E_x^s = 0$ , so that the field contains a single linearly polarized transverse component  $E_z^s$  (as was supposed in the main text) and, probably, the longitudinal component  $E_y^s$  (note that the condition  $E_x^s = 0$  is not critical, and the same reasoning can be reproduced for non-zero  $E_x^s$ ). Then, Equation A2 reduces to

$$\frac{\partial^2 E_z^s}{\partial x^2} + \frac{\partial^2 E_z^s}{\partial y^2} + k^2 \epsilon E_z^s = \frac{\partial^2 E_y^s}{\partial z \partial y}, \quad \frac{\partial^2 E_y^s}{\partial x^2} + \frac{\partial^2 E_y^s}{\partial z^2} + k^2 \epsilon E_y^s = \frac{\partial^2 E_z^s}{\partial z \partial y}. \quad (\text{A3})$$

Note that the “pure” 2D model is described by the 1<sup>st</sup> Equation A3 with zero r.h.s., and our present task is to estimate this “perturbing” r.h.s.,  $\partial^2 E_y^s / \partial z \partial y$ . To this end we recall that, according to Equation 1, all components contain rapidly oscillating multipliers like  $\exp(-iky)$ , due to which an asymptotic relation takes place:  $\partial/\partial y \sim -ik$ . Further, let the SC bases (end faces) be situated in planes  $z = \pm h/2$ , i.e., its length (distance between the forward and backward

ends) equals to  $h$ , and we consider the field in the middle plane  $z = 0$ , equally removed from both ends. In this situation, the derivatives with respect to  $z$  also obey an asymptotic relation, now of the form  $\partial/\partial z \lesssim 1/h$ . Taking into account that the  $x$ -sizes of the field inhomogeneities in calculated examples (Figures 2–7) are less than the wavelength, the relation  $\partial/\partial x \gtrsim 1/\lambda \sim k$  can be safely accepted. Then, the magnitude of the l.h.s of the second Equation A3 can be estimated as  $\sim k^2 E_y^s$  while estimation of its r.h.s. gives  $\sim (k/h) E_z^s$ . Therefore, from the correspondence  $k^2 E_y^s \sim (k/h) E_z^s$ , the asymptotic relation follows between  $E_y^s$  and  $E_z^s$ :

$$E_y^s \sim (kh)^{-1} E_z^s. \quad (\text{A4})$$

This is a reasonable evaluation of the strength of the longitudinal component of the PMJ field. After substitution of this result into the r.h.s. of the 1<sup>st</sup> Equation A3, we find that this r.h.s. is of the order  $\sim h^{-2} E_z^s$ , whereas its l.h.s. is  $\sim k^2 E_z^s$ . In other words, the r.h.s. of the 1<sup>st</sup> Equation A3, supplying the corrections for the finite SC length, is of the order of  $(kh)^{-2}$  with respect to the “main” l.h.s. Accordingly, the expression  $(kh)^{-2}$  quantifies the possible relative errors associated with the restricting to a “pure” 2D model (with discarded r.h.s. of the 1<sup>st</sup> Equation A3). For example, if  $\lambda = 1310$  nm and  $h = 6$   $\mu\text{m}$ ,  $kh = 28.8$ , and  $(kh)^{-2} \approx 0.0012$ . This means relative errors at the level of 0.1%, which is not critical for the meaningful interpretation of the results and their discussed applications.

Of course, the above reasonings are essentially based on the presumption that the field is considered far from the sharp boundaries where  $\epsilon$  is discontinuous, and spatial derivatives of the field components may increase dramatically. If the considered points deviate from the SC middle section or approach close to its surface (reaching the distances  $\lesssim \lambda$ ), the picture will be much less favorable. Nevertheless, there are wide areas of the  $(x, y)$ -plane where the 2D approximation describes the transverse cross section of the SC-generated PMJ with accuracy sufficient for many applications.